Simple lattice-dynamical slab model for interpreting surface vibrational spectra: Application to oxygen on Ni(100) and Ni(111)

R. L. Strong and J. L. Erskine
Department of Physics, University of Texas, Austin, Texas 78712
(Received 10 September 1984)

A parametrized lattice-dynamical slab model is presented and used to analyze the vibrational properties of oxygen adsorbed on Ni(100) and Ni(111) surfaces. Results obtained from the slab-model technique are compared with corresponding predictions based on a Greens's-function approach to contrast the relative merits of these two methods for obtaining information about vibrational phenomena. The lattice-dynamical slab model is also used to analyze experimental data for several ordered oxygen configurations on the Ni(111) and Ni(100) surfaces, including the proposed pseudobridge site for $c(2\times2)$ oxygen on Ni(100). The results presented indicate that lattice-dynamical calculations can be used not only to test structural models proposed on the basis of experimental measurements or other theoretical calculations, but can also serve as a basis for independent structural determinations (bonding sites and bond lengths) when there is sufficient surface vibrational data to constrain the calculations adequately.

INTRODUCTION

The study of surface vibrations of crystals and adsorbates on crystal surfaces represents one of the more rapidly growing areas of surface physics. Intense interest in this subject and the rapid growth of the work in this area has been stimulated by recent advances in experimental techniques, which permit a complete characterization of surface phonons throughout the two-dimensional Brillouin zone, as well as improvements in numerical methods for calculating surface vibrational phenomena. Inelastic molecular-beam scattering[1] has yielded surface-phonon dispersion curves for low-index faces of the alkali halides as well as some noble metals.[2] Inelastic electron scattering from surfaces, which is most commonly referred to as electron-energy-loss spectroscopy (EELS), has refined our understanding of the scattering processes which underlie electron scattering from surface vibrations, and has also produced full phonon dispersion curves for clean Ni(100) surfaces[3] and several ordered overlayer systems.[4,5]

A complete characterization of inelastic scattering of atoms or electrons from surfaces requires an integrated treatment of both the scattering process and the dynamics of the scattering system. However, one of the most attractive features of inelastic scattering spectroscopies such as neutron scattering, atom scattering, and EELS is that detailed information related to structure, bond distances, and interatomic force constants can be obtained directly from the kinematic conditions for scattering[4] (energy- and momentum-conservation laws). Kinematic conditions constrain the scattering parameters which can result from a given scattering system and incident particle. Conversely, when the scattering properties of a given system have been accurately determined from a broad range of scattering parameters, the results can be used to obtain information about the scattering system using appropriate models. The site, height, and force constants associated with an adsorbed atom on a surface directly affect the vibrational modes associated with that adsorbed atom as well as the surface-phonon modes of the substrate. It is reasonable to assume that structural parameters, i.e., the adsorbate height as well as the force constants, could be determined from the vibrational properties of the surface complex provided the vibrational spectra were known and an appropriate model connecting the various constants and the vibrational modes were available.

Low-energy electron diffraction (LEED) is unquestionably the most useful and widely used technique for determining surface structure. Structure determination based on LEED requires difficult multiple-scattering calculations,[6,7] and there are many surfaces (for example, the reconstruction on silicon) for which the structure has not yet been established. There are even examples of simple adsorbate systems in which LEED studies have encountered difficulty in obtaining a single structural parameter such as an adsorbate bond height. Two specific examples are O/Al(111) (Ref. 8) and $c(2\times2)$O/Ni(100) (Ref. 9). In the O/Al(111) system, the problem is that the initial stage of oxygen chemisorption on Al(111) involves simultaneous formation of overlayers and underlayers. This property was directly evident in EELS studies[10] but was not evident in LEED, therefore the initial attempts to determine the oxygen-bond distance using LEED failed because the calculations were based on the incorrect assumption that the chemisorbed configuration involved only an overlayer. The EELS measurements[10] and lattice-dynamical calculations,[11] similar to those discussed in this paper, were able to determine that overlayer and underlayer oxygen formed simultaneously, and also established that a temperature of 300 K was sufficient to initiate and sustain the underlayer formation on Al(111) after oxygen adsorption. The $c(2\times2)$O/Ni(100) appears to be a case in which at least two oxygen-bond distances yield nearly equivalent R factors for LEED calculations and, in addition, a lower-

symmetry surface site termed the pseudobridge site apparently yields an even better R factor.[12] This is a second example where LEED alone has failed to yield an unambiguous determination of a surface-structure parameter. Based on these examples, it is clear that independent alternatives for surface-structure determination are needed. Surface vibrational spectroscopy provides one such alternative.

This paper discusses application of lattice-dynamical slab calculations to obtain structural parameters from the results of electron (EELS) or atom scattering experiments which only rely on kinematic conditions for their interpretation. These experiments yield the surface vibrational modes of the surface complex. It should be mentioned here that techniques for probing surface structure based on the energy dependence of inelastic scattering cross sections[13] are also being investigated both experimentally and theoretically. These investigations may yield an independent approach for structural determination based on inelastic electron scattering. In the present paper, we will show that lattice-dynamical slab calculations can unambiguously determine overlayer structural parameters by fitting the dispersion curves of the surface vibrational modes. These dispersion curves are found from the vibrational data using only the kinematic scattering conditions for their determination.

FINITE-SLAB MODEL

The two most common techniques for calculating vibrational spectra are the finite-slab and the Green's-function method for a semi-infinite slab. The Green's function calculations "involve considerable complexity in both algebra and numerical computation by computer."[14] The finite-slab method has the advantages of fast computation and straightforward implementation, and it is easy to adapt to different crystal geometries. The Green's-function method has the apparent advantage of continuous rather than discrete spectral densities but, as will be shown, this difference is hardly significant. In both methods the physical model is the same or similar, often based on nearest-neighbor central forces in the harmonic approximation. However, in the Green's-function calculations it is assumed that below a certain layer (e.g., the third or fourth substrate layer) the Green's function obey an exponential decrease with increasing depth beneath the surface.[5] No similar assumptions are necessary in the finite-slab calculations. As the calculations of Allen *et al.*[15] have shown, the actual variation of vibrational amplitude with layer depth can be extremely complex. Our calculations reveal that many of the normal modes of a finite slab are "antisurface" modes, with little or no vibrational amplitude at the surface increasing to a constant amplitude as the center of the slab is approached, similar to the function $1-e^{-z}$, where z is zero at the surface and increases as z increases into the crystal.

Our finite-slab model is a modification of the model used by Allen *et al.*[15] The computer code was provided to us by F. W. deWette and B. Firey and was modified to permit more convenient numerical calculation of the surface lattice-dynamical properties of ordered overlayers on crystal surfaces. The basic lattice-dynamical model is formulated for nonionic crystals after Maradudin *et al.*[16] Our implementation of the model is described in this section and in the Appendix. Input parameters which must be specified in order to execute a calculation include the position, mass, and "type" of each atom in the unit cell of the slab and a complete description of the force constants or potentials which characterize the pair interactions. The slab calculation returns eigenvalues and eigenvectors representing a complete characterization of the lattice dynamics of the slab.

In this paper, we will show that when sufficient experimental data are available to characterize the surface lattice-dynamical behavior of an adsorbate substrate system, an iterative procedure can be used to determine accurately the input parameters for which the model yields the best fit to experimental results. The sensitivity and accuracy of this procedure is sufficient to determine structural parameters, in particular the bond distance of an adsorbed overlayer.

The calculational procedure begins by defining a slab unit cell which is based on the periodicity of the ordered adsorbate layer and extends throughout the thickness of the slab. A type parameter is used to distinguish atoms of different elements and possibly atoms of the same element located in unequivalent lattice sites within the unit cell. For example, if the surface is reconstructed the force constants at the surface could be different from those in the bulk, so surface atoms can be distinguished from bulk atoms using the type parameter. The type parameter thus allows different kinds of atom pairs to be distinguished, so that each inequivalent pair can be assigned a different pair potential (force constant). The crystal structure (e.g., face-centered cubic), crystal face (100 111, etc.), and overlayer periodicity are varied by changing the atom's coordinates in the unit cell and the two primitive translation vectors parallel to the surface.

The user also specifies the finite range and strength of the central-force pair potentials and the value of the two-dimensional wave vector $\mathbf{q}_{||}$ in reciprocal space. If desired, three-body angle-bending interactions may also be included in the calculation (we have used a Keating potential[17] for our adsorbate angle-bending interactions). Since every atom should be at static equilibrium, we chose each pair potential so that the atoms in the pair are in static equilibrium with respect to each other. After Allen *et al.*,[15] we used the Lennard-Jones 6-12 potential

$$\phi(r)=4\epsilon[(\sigma/r)^{12}-(\sigma/r)^{6}]\ , \tag{1}$$

where r is the distance between atoms, ϵ is the interaction strength, $\sigma=2^{-1/6}r_0$, and r_0 is the equilibrium distance between the atoms. With this potential the radial central-force constant is $72\epsilon/r_0^2$, so the force constant can be changed by varying r_0 or ϵ. In general only first-nearest-neighbor interactions are included, but as many neighbors as desired can be included by using different values of ϵ for different distances between atoms. With only first-nearest-neighbor interactions the Lennard-Jones model and a force-constant model are equivalent except in the latter case the force constants are not altered when distances between atoms are varied. We have used the

Lennard-Jones potential in calculations involving substrate interactions up to seventh nearest neighbors using a single value of ϵ for all substrate interactions, with $\sigma_{\text{substrate}}=0.91712 r_{\text{NN}}$ to minimize the static energy of the slab[15] (r_{NN} is the nearest-neighbor substrate distance). Although in these calculations the atoms in the slab are not in static equilibrium, the quantitative results of the seventh-nearest-neighbor calculations are almost identical to the first-nearest-neighbor calculations due to the rapid decrease in ϕ as r is increased (i.e., the first-nearest-neighbor substrate interaction greatly dominates the other substrate interactions).

The computer first generates the dynamical matrix by summing over all pairs of atoms involving one atom in the primary unit cell and another atom (possibly inside the primary unit cell) within the maximum chosen interaction length of the primary unit cell. The computer then determines the eigenfrequencies and eigenvectors for all of the normal modes of vibration of the slab (refer to Appendix). Based on the computed eigenvectors, surface and bulk phonon modes are identified, and dipole- and impact-scattering spectral densities are determined for each eigenfrequency. To determine which modes are surface modes we compare the sum of the squares of the vibrational amplitudes in direction $\alpha(=x,\ y,$ or $z)$ of the substrate atoms inside the unit cell in a given layer. The slab center is not used since in some of the eigenmodes the center layer has twice the amplitude it would have if there were only one surface to the slab due to the superposition of the contributions from each slab surface. It is usually necessary to skip one layer between comparisons because of the relative motion of atoms in adjacent layers. In most eigenmodes, when one layer is vibrating in the direction perpendicular to the surface the layer above and below it are vibrating parallel to the surface. If each layer were compared with the layer immediately below it, most surface modes would not satisfy our criterion that the amplitude decrease in all three directions simultaneously, but when alternate layers are compared the known surface modes meet the criteria, justifying its definition.

It should be noted that if the slab is less than 13 layers thick (because of computer-memory limitations), there are not enough layers to compare in one half of the slab to totally characterize all the modes as being bulklike or surfacelike, but the criteria still decrease the number of possible surface modes considerably (many bulk modes can be identified, but some bulk modes are incorrectly assigned as surface modes due to an insufficient number of layer comparisons). It is possible for modes to meet the criteria in one or two directions but not all three. When the criteria are met in only two directions the eigenvectors are visually inspected to determine if the mode should be considered a surface mode, since one layer-to-layer comparison is sufficient for the computer to assign a mode as being bulklike in a particular direction. In almost all cases the third direction displays bulklike eigenvectors and the mode is not a true surface mode. A mode which fails the test in all three directions is definitely a bulk mode; if it fails in one or two directions it could be a bulk mode or a surface-resonance mode (a special type of bulk mode which will be discussed later), depending on the value of its spectral densities (bulk modes have zero dipole and impact spectral density while surface-resonance modes do not).

These criteria were arrived at empirically, by examining the eigenvectors of the fcc(100) surface and an fcc(111) surface where the stacking patterns are *ABAB*. . . and *ABCABC*. . . . On the (100) surface the alternate layers are of the same type, but on the (111) surface they are not. If on the fcc(111) surface one compares *A* layers with *A* layers and *B* layers with *B* layers, one cannot correctly identify the surface modes. However, by comparing alternating layers, the surface modes are identifiable with any stacking sequence.

The effective dipole spectral density in direction α for two-dimensional wave vector $\mathbf{q}_{||}$ and ith eigenfrequency $\omega_i(\mathbf{q}_{||})$ is

$$\rho^{D}_{i\alpha}(\mathbf{q}_{||})=\frac{\left|u_{i\alpha}(\mathbf{q}_{||}\mid \text{ads},0)-\frac{1}{N}\sum_{\text{sub}}\sum_{l}u_{i\alpha}(\mathbf{q}_{||}\mid \text{sub},l)\right|^2}{1-e^{-\hbar\omega/k_B T}}, \tag{2}$$

where $u_{i\alpha}(\mathbf{q}_{||}\mid k,l)$ is the α component of motion of atom k (adsorbate or substrate) in unit cell l in the corresponding ith eigenmode and the sums are over the adsorbate's N-substrate nearest neighbors, some of which may be in different unit cells from the adsorbate. The denominator is due to the factor $1+n(\omega)$ in the formula for the scattering cross section,[18] where $n(\omega)$ is the Bose-Einstein distribution factor. It is assumed that the effective charge on the adsorbate's nearest substrate neighbors is distributed equally, and that the total substrate effective charge is opposite the effective charge of the adsorbate to ensure charge neutrality of the system. The average component of the displacement of all of the adsorbate's nearest-neighbor substrate atoms, both inside and outside the unit cell, is used instead of an average over only those atoms inside the unit cell (as proposed by Mills *et al.*[5,18,19]) so that the choice of unit cell does not affect the symmetry of the dipole spectral density with respect to the group symmetry of the adsorbate substrate system. For example, Mills's formulation of the dipole spectral density produces drastically different results for $c(2\times2)$O/Ni(100) when $\mathbf{q}_{||}$ is parallel and perpendicular to the two nickel atoms chosen to be inside the unit cell, corresponding to two equivalent points along $\bar{\Delta}$ (the line from $\bar{\Gamma}$ to $\bar{X}$), while our spectral density is identical for both directions of $\mathbf{q}_{||}$. This results from the plane-wave nature of the atomic displacements, with equivalent atom's motions related by

$$u_{i\alpha}(\mathbf{q}_{||}\mid k,l)=u_{i\alpha}(\mathbf{q}_{||}\mid k,0)e^{i\mathbf{q}_{||}\cdot\mathbf{R}_{||}(l)}, \tag{3}$$

where $\mathbf{R}_{||}(l)$ is the two-dimensional translation vector from cell 0 to cell l. Consequently, if $|\mathbf{q}_{||}|\neq0$ the atoms outside the unit cell are not in phase with the atoms inside the unit cell (unless $\mathbf{q}_{||}=\mathbf{G}$, where $\mathbf{G}$ is a reciprocal-lattice vector), and it is exactly this phase relationship which determines the average displacement of the substrate atoms, as well as the dipole spectral density. If $|\mathbf{q}_{||}|=0$ ($\bar{\Gamma}$) or all of the adsorbate's substrate nearest

neighbors are inside the unit cell, Mills's formulation of the dipole spectral density is valid. It is not immediately clear what effect this difference has on the dispersion curves calculated by Rahman *et al.*[5] for $c(2\times2)$O/Ni(100) with dipole-dipole interactions included, but the discrepancy will be smallest at $\bar{\Gamma}$ (since the substrate atoms outside the unit cell are in phase with the corresponding atoms inside the unit cell) and largest at $\bar{X}$ [the substrate atoms on opposite sides of the adsorbate atom are 180° out of phase in a $c(2\times2)$ unit cell, so the contribution of the substrate atoms to the dynamic dipole moment should be zero]. Our calculated frequency spectra are identical at equivalent points in the surface Brillouin zone independent of the definition of the dipole spectral density.

The effective-impact spectral density is taken to be

$$\rho^{I}_{i\alpha}(\mathbf{q}_{||})=\frac{\sum_{k}|u_{i\alpha}(\mathbf{q}_{||}|k,0)|^{2}}{1-e^{-\hbar\omega/k_{B}T}}, \tag{4}$$

where k is an adsorbate or surface-substrate atom inside the unit cell, since it is assumed that all atoms at the surface have an equal probability of impact scattering the incident electrons, and the scattering cross sections are approximated by the kinematic quantity $|k_{\alpha}u_{i\alpha}(\mathbf{q}_{||}|k,l)|^{2}$ for scattering in direction α, where k_{α} is the α component of the wave vector of the incident electron. This is essentially a superposition of the adsorbate spectral density in direction α with the substrate spectral density in direction α, with a weighting factor to reflect the adsorbate coverage of the surface. Modes which have little or no dipole spectral density in direction α can have a large-impact spectral density, and the dipole spectral density is really only valid near $\bar{\Gamma}$. By computing both spectral densities, it is possible to determine which modes might be observable at any point in the surface Brillouin zone.

By determining the surface modes and the spectral densities, the calculations immediately reveal the dominant surface polarization and intensity of each eigenmode. This greatly facilitates interpretation of the calculation and correlation with the experimental data and allows the user to see quickly the effect on the surface modes of varying one of the parameters. Eigenmodes with large spectral densities which are not surface modes must be bulk modes and consequently appear in clusters with a small energy spread. These are the so-called surface-resonance modes. A very simple test to determine if an eigenmode is a true surface mode or if it belongs to a surface resonance is to change the number of atoms in the slab by varying the slab thickness. If the spectral densities do not change, the mode is a true surface mode. Otherwise the mode belongs to a surface resonance (see Fig. 1). Bulk modes which are not resonance modes have zero spectral density and constitute the majority of the modes.

With a 28-atom unit cell and only nearest-neighbor central forces the program requires 7 seconds of CPU time on a Control Data Corporation (CDC) Dual Cyber 1/0/750 (125 seconds of CPU time on a VAX 11/780) for one value of $q_{||}$, allowing numerous iterations to be performed fairly rapidly while adjusting parameters to fit the data. Once a best fit has been obtained, more detailed results can be obtained if desired by increasing the slab thickness and correspondingly the running time (a 56-atom unit cell requires less than 2 minutes of CPU time on the Cyber and 23 to 24 minutes of CPU time on the VAX). The only limitation to the application of the model is the requirement that the user must have some idea of the value of the substrate's bulk nearest-neighbor force constant or know the bulk maximum phonon frequency of the single crystal (usually available from neutron or x-ray diffraction experiments), since the substrate force constant can be determined by fitting the maximum calculated frequency of the substrate to this frequency. This limitation applies to the Green's-function method as well. The validity of the model will be demonstrated with the system O/Ni(111), and results for O/Ni(100) will be discussed.

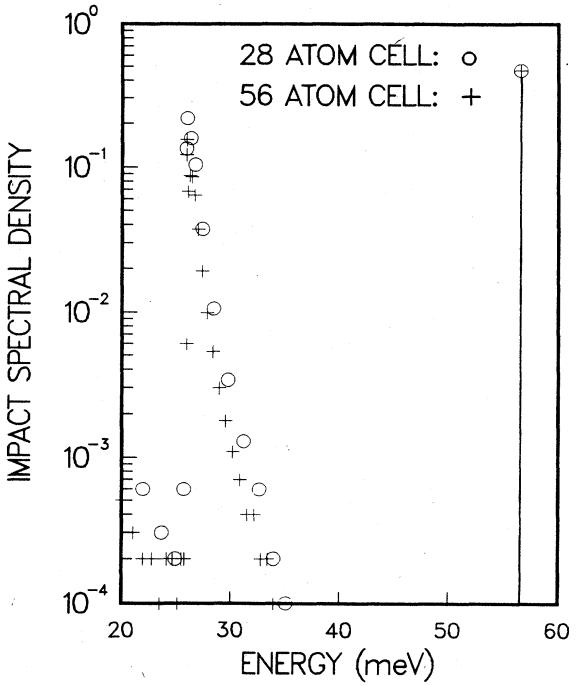

FIG. 1. Impact-spectral density of $c(2\times2)$O/Ni(100) at $\bar{\Gamma}$ for vibrational motion parallel to the surface and in the scattering plane. The oxygen is located in the fourfold hollow sites at a height of 0.92(224) Å and the surface is relaxed outward 5.2%. Open circles are results of a 13-substrate-layer slab calculation with 2 adsorbate layers and 28 atoms per unit cell, while plus signs are from a 27-substrate-layer slab calculation with 2 adsorbate layers and 56 atoms per unit cell. Note that the two spectral densities are identical for the oxygen mode parallel to the surface near 56 meV (a true surface mode), while the spectral densities for the 27-layer slab are lower in the collection of modes peaked near 25 meV (a surface-resonance mode).

EXPERIMENTAL RESULTS

Adsorbate vibrational spectra can be measured by several different techniques, each with its own advantages and disadvantages, but EELS appears to be the best suited for measuring vibrational energies from 0—500 meV and is capable of detecting vibrations both perpendicular and

parallel to the surface. In EELS a monochromatic beam of electrons (0—300 eV kinetic energy) is reflected from the sample surface and energy analyzed to detect the amount of energy the electrons have lost (or gained) in exciting (deexciting) vibrational quanta. Conservation of energy requires that the incident and scattered electron kinetic energies E_i and E_s are related to the frequency ω of the vibrational mode excited by $E_s = E_i - \hbar\omega$. Conservation of wave vector parallel to the surface requires that $\mathbf{k}_{s\|} = \mathbf{k}_{i\|} - \mathbf{q}_{\|} - \mathbf{G}$, where $\mathbf{k}_{s\|}$ and $\mathbf{k}_{i\|}$ are the projection of the scattered and incident electron wave vectors onto the surface plane ($k_{\|} = k \sin\theta$, where θ is measured from the surface normal), $\mathbf{q}_{\|}$ is the phonon's wave vector parallel to the surface, and $\mathbf{G}$ is a two-dimensional reciprocal-lattice vector. The electron's energy and wave vector are related by $|\mathbf{k}| = 0.512\ \text{Å}^{-1}\sqrt{E(\text{eV})}$, so $\mathbf{q}_{\|}$ can be varied by changing the incidence angle or scattering angle of the electrons along with the incident kinetic energy. These kinematic scattering laws allow the dispersion of vibrational-mode energies with wave vector to be determined from the experimental data.

Our EELS experiments were performed with a Leybold-Heraeus ELS-22 spectrometer with a 127° sector double-pass monochromator and double-pass analyzer. The electron optics were modified by adding an additional lens on both the monochromator and analyzer sides, permitting incident energies up to 300 eV.[4] The nickel crystal, purchased from Leico, was spark cut from a 3/8-in.-diam rod after aligning to within ±1° by x-ray diffraction. After polishing to a mirror finish with 1μ alumina powder, the sample was cleaned *in situ* by sputtering with 500- or 1000-eV argon ions at a pressure of 5×10^{-5} Torr while heating the sample resistively to 800 K or higher. Sample cleanliness was checked by Auger electron spectroscopy using a Physical Electronics double-pass cylindrical mirror analyzer. A Varian four-grid LEED optics system was used to check that the cleaned surface was well ordered before admitting gas to form adsorbed layers and to determine the adsorbate periodicity after exposure (accomplished by back filling the vacuum chamber to between 10^{-9} and 10^{-6} Torr, as determined by a nude ionization gauge). The $c(2\times2)$O overlayer was formed at approximately 500-K sample temperature, measured by a chromel-alumel thermocouple spot welded to the edge of the crystal, while monitoring the LEED pattern for the disappearance of the $(0,\frac{1}{2})$ LEED spots characteristic of the $p(2\times2)$ overlayer.

Incident electrons can interact with the substrate (and adsorbate, if present) through long-range dipole scattering[18] or short-range impact scattering.[13] Dipole scattering is sharply peaked around the specular direction (scattering angle equals incident angle) while impact scattering is broadly distributed over all scattering angles. In specular geometry the dipole selection rule[18] restricts the observable vibrational modes to those having a nonzero dipole moment perpendicular to the surface. In off-specular geometry impact-scattering selection rules[13] determine which surface vibrational modes are observable. Typically, if the scattering plane is along a mirror plane, surface vibrational modes which are even under reflection in the mirror plane should be observable while those which are odd under reflection should not be observable. Vibrational modes lacking any sort of mirror symmetry should also be observable since the symmetry arguments used to derive the selection rules cannot be applied. The observation of vibrations polarized parallel to the surface or the measurement of the dispersion of vibrational modes along crystallographic directions necessitates use of the impact-scattering mechanism. Therefore, the most useful experiments must be performed in off-specular geometry and at fairly high kinetic energies. Figures 2—4 display typical specular and off-specular EELS spectra for $c(2\times2)$O/Ni(100), reflecting the difference in counting rates associated with the two scattering mechanisms.

SLAB-MODEL CALCULATIONS

There has been some concern regarding the ability of a finite-slab calculation to produce an accurate spectral density because of the discrete nature of the calculation.[20] It has been postulated that delta-function-like features which appeared below the maximum bulk phonon frequency in the continuous spectral density calculated by the Green's-function method could fall in between the discrete lines calculated by the finite-slab method, since a unit cell with N atoms would have only $3N$ modes distributed in frequency (over approximately 39 meV in the case of nickel).

Since the Green's-function method had been used to

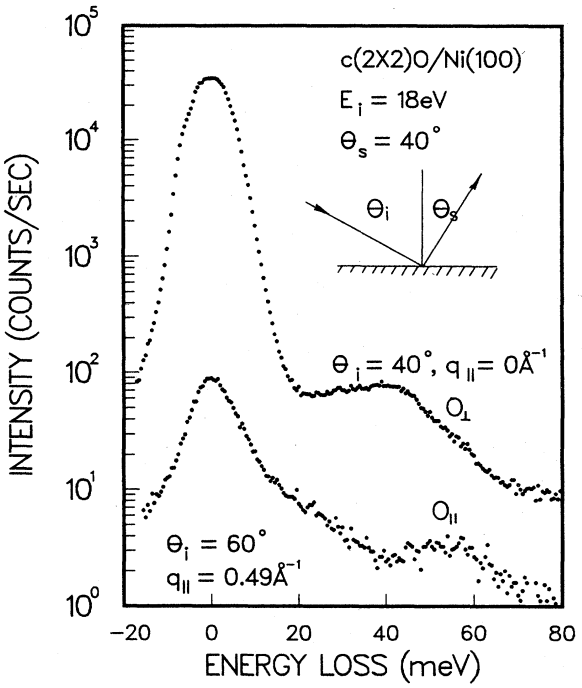

FIG. 2. Electron-energy-loss spectra for $c(2\times2)$O/Ni(100). θ_i and θ_s are the incident angle and scattering angle, respectively, of the electrons measured from the surface normal. The incident electron kinetic energy is E_i. The oxygen mode perpendicular to the surface is observed in specular geometry ($\theta_i = \theta_s$), and the oxygen mode parallel to the surface is observed in off-specular geometry ($\theta_i \neq \theta_s$).

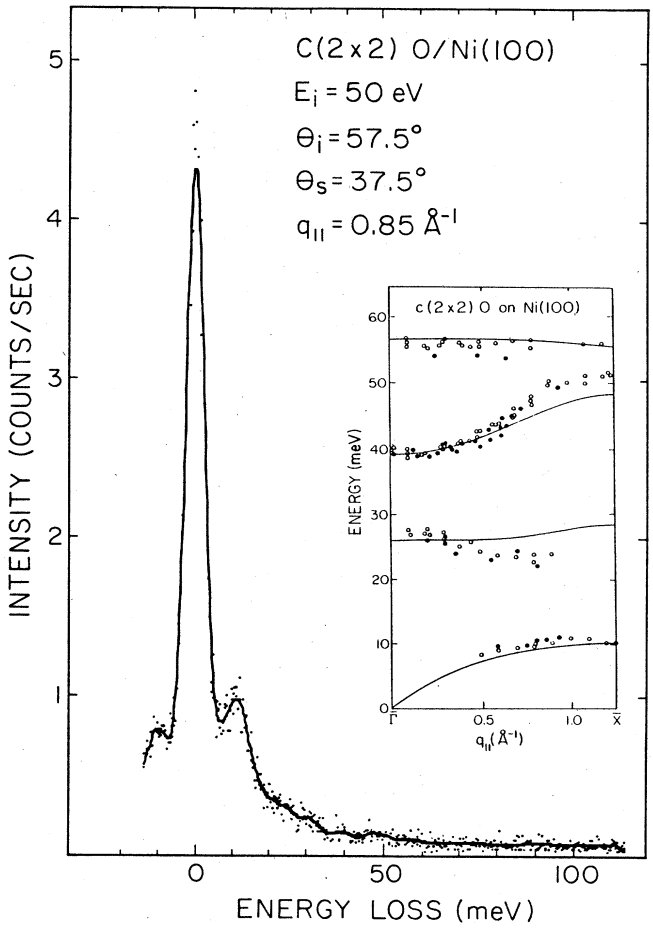

FIG. 3. Electron-energy-loss spectrum for $c(2\times2)$O/Ni(100) displaying the S_4 surface-phonon gain and loss peaks. Inset shows surface-mode dispersion curves measured along $\bar{\Delta}$ with solid circles representing our data and open circles representing data of Szeftel *et al.* (Ref. 26). Solid lines are our calculated dispersion curves fit to one or two points on each of the measured dispersion curves.

determine the adsorbate site of oxygen in the system $(\sqrt{3}\times\sqrt{3})R\,30°$ O/Ni(111) (Ref. 20) at $\bar{\Gamma}$ corresponding to the specular EELS data of Ibach and Bruchmann,[21] we chose to test our finite-slab model on this system and to address the issue regarding the accuracy of discrete spectral densities determined using slab-type calculations. Low-energy electron diffraction has determined the height of the oxygen above the surface for this system but apparently cannot determine in which of the two inequivalent threefold hollow sites the oxygen is adsorbed.[22] The Ibach-Bruchmann EELS data reveal two features (see Fig. 5), one above the nickel bulk phonon maximum and the other below. Based on the dipole selection rule, it is assumed that these two modes observed in specular scattering geometry are polarized perpendicular to the surface (the z direction) and that the higher mode corresponds to the atomic vibration of the oxygen atom. The continuous dipole spectral density calculated by the Green's-function method[20] with nearest-neighbor central forces predicts two z-polarized modes for the fcc site and

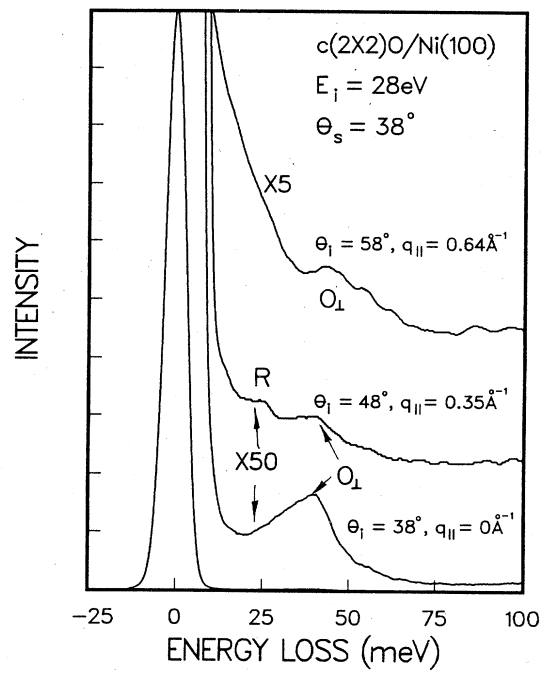

FIG. 4. Electron-energy-loss spectra for $c(2\times2)$O/Ni(100) displaying the dispersion of the oxygen mode polarized perpendicular to the surface as well as the surface-resonance mode R near 25 meV.

three for the hcp site, indicating adsorption at the fcc site (the fcc site is above a third-layer nickel atom while the hcp site is above a second-layer nickel atom). The Green's-function calculations fit the high-energy peak at

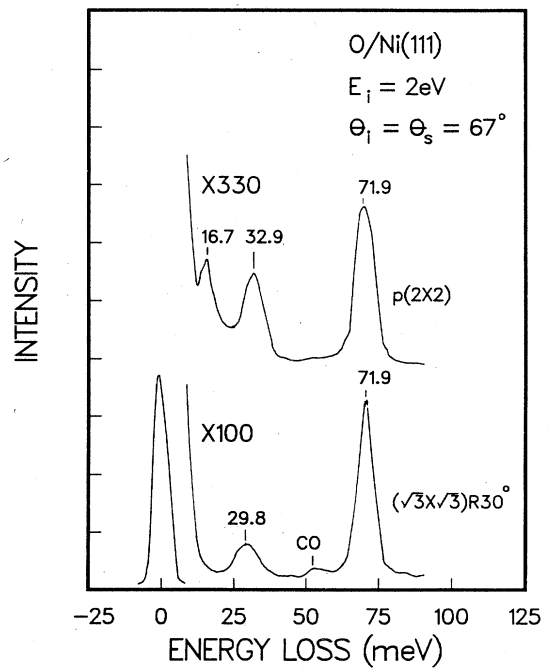

FIG. 5. Electron-energy-loss spectra for O/Ni(111) reported by Ibach and Bruchmann (Ref. 21). The upper curve corresponds to a $p(2\times2)$ overlayer and the lower to a $(\sqrt{3}\times\sqrt{3})R\,30°$ overlayer.

71.9 meV and the lower-energy peak was calculated 2.9 meV lower than observed. Our finite-slab calculation using first-nearest-neighbor central forces and fitted to the high-energy peak gives discrete dipole spectral densities having peak energies which are nearly identical to those of the continuous dipole spectral density for each site (see Fig. 6). The differences in shape and intensity of the discrete and continuous spectral density is probably due to differences in definitions of the spectral density (the authors define several different spectral densities in this paper[20] and do not make it clear which one is used in the figures). Also, the discrete spectral density would have to be made continuous by Gaussian broadening or by convoluting it with an appropriate function to imitate the instrumental response function of the EELS spectrometer. In both our finite-slab and the Green's-function calculations[20] the height of the oxygen atom was fixed at the value determined by LEED,[22] or by *ab initio* cluster calculations,[23] the substrate was terminated assuming no surface reconstruction, and the nickel-oxygen first-nearest-neighbor central-force constant was the single parameter to fit the spectra (after fitting the maximum bulk phonon frequency with the nickel-nickel neighbor central-force constant). Both models are essentially the same except in the method that the spectral densities are calculated. As a further test of our calculational procedures, our finite-slab model was applied to the $p(2\times2)$ overlayer of O/Ni(111), for which Green's-function calculations have not been published. Ibach's EELS data[21] reveal the same high-energy peak but two different low-energy peaks. Our finite-slab calculation fitted to the high-energy peak yields two low-energy modes for the fcc site which agree with the data to within 1.3 meV (although the lowest-energy mode at 15.9 meV is anomalously weak), while the hcp site is 13 times less intense than the fcc site in the 15.9 meV peak (see Fig. 7). This result suggests that the oxygen atoms prefer the fcc threefold hollow sites for both overlayers.

The calculations just described were performed at $\bar{\Gamma}$ us-

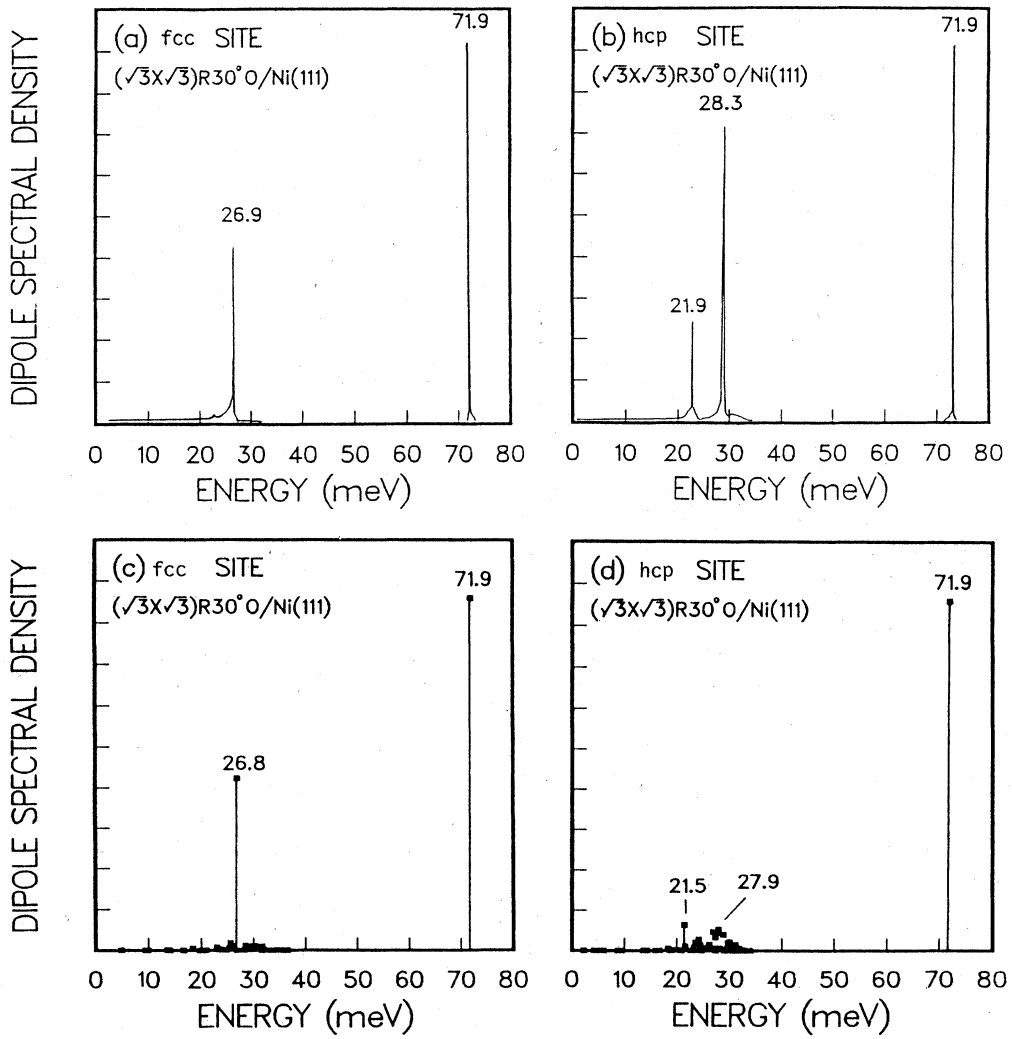

FIG. 6. Continuous (Ref. 20) [(a) and (b)] and discrete [(c) and (d)] dipole spectral densities for $(\sqrt{3}\times\sqrt{3})R30°$ O/Ni(111), with the oxygen adsorbed in the fcc [(a) and (c)] or hcp [(b) and (d)] threefold hollow sites. The fcc site is above atoms in the third nickel layer while the hcp site is above atoms in the second nickel layer.

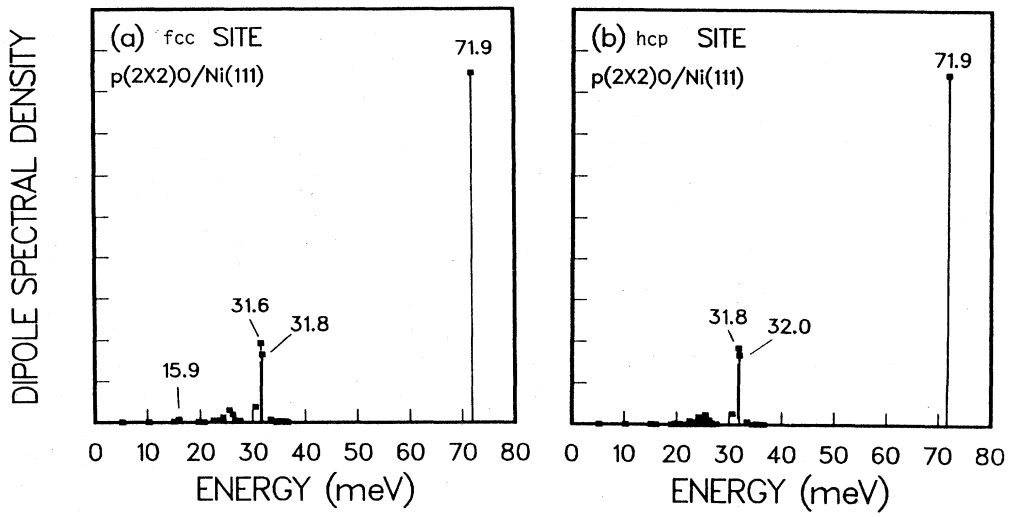

FIG. 7. Discrete dipole spectral densities for $p(2\times2)$O/Ni(111), with the oxygen adsorbed in the fcc (a) or hcp (b) threefold hollow sites.

ing an experimentally determined height for the adsorbate atom. It is a trivial matter to perform the finite-slab calculations away from $\bar{\Gamma}$, while it appears to make the Green's-function calculations more difficult. The adsorbate height need not be known, and, in principle, can be determined from the model if there is sufficient experimental data, namely, the adsorbate vibrational modes both perpendicular and parallel to the surface, to serve as constraints on the model as the adsorbate height and other parameters are varied. For $c(2\times2)$O/Ni(100) this data is now available. Previously, *ab initio* cluster calculations[23] and lattice-dynamical Green's-function calculations[19] correctly predicted the frequency at $\bar{\Gamma}$ of the oxygen mode perpendicular to the surface, but concluded that the oxygen height was 0.26 Å while LEED[24] and other experimental techniques[25] indicated the height was approximately 0.9 Å. Additional LEED calculations[9] revealed two minima in the R factor of similar value at 0.0 and 0.9 Å, so LEED proved unable to unequivocably determine the adsorbate height. EELS data taken in off-specular geometry (away from $\bar{\Gamma}$) characterized the oxygen mode parallel to the surface as well as two surface modes below the nickel bulk phonon maximum. The dispersion curves from $\bar{\Gamma}$ to $\bar{X}$ for these four modes have been published by Szeftel *et al.*[26] and are consistent with our own data acquired prior to their publication (see Fig. 3). Rahman *et al.*[5,26] calculated the dispersion of these modes using the Green's-function method assuming adsorption in the fourfold hollow site at heights of 0.9 and 0.26 Å with a three- and four-parameter fit, respectively. Rahman *et al.* did not otherwise vary the height to achieve a best fit to the dispersion curves. The agreement with experiment was significantly better with the oxygen at 0.9 Å, but it is not evident from their calculations that some other oxygen height would not fit the data as well or better. Nor is it clear what effect variation of other relevant parameters would have on the various modes. Some features of the dispersion curves and the effect on the dispersion curves of varying certain force constants are said to be obvious, but Rahman *et al.* do not offer any substantiation for these statements or fully explore all of the relationships which might exist. With the finite-slab model it is possible to perform numerous calculations in a short time in order to investigate all desired parameters thoroughly, including the effect of varying the adsorbate height.

We have performed a seven-parameter finite-slab calculation using the data of Szeftel *et al.*[26] for a common reference. The calculations were fit to the oxygen parallel mode frequencies at 0.3 and 0.8 Å^{-1} away from $\bar{\Gamma}$ along $\bar{\Delta}$, the oxygen perpendicular mode and surface-resonance mode frequencies at 0.3 Å^{-1}, and the S_4 surface-phonon frequency at 1.26 Å^{-1} ($\bar{X}$). The parameters are the height of the oxygen atom above the surface, the nickel-oxygen-nickel angle-bending force constant, the second-nearest-neighbor nickel-oxygen interactions strength, and the following first-nearest-neighbor interaction strengths: nickel-oxygen, oxygen-oxygen, (surface nickel)-(surface nickel), (surface nickel)-(second-layer nickel). The best fit occurred with no angle-bending forces and no second-nearest-neighbor interactions, so there were effectively five parameters to fit to five data points (more data points could have been included if necessary). The outer nickel layer was relaxed outward 5.2% based on Rutherford backscattering data.[27] However, variation of the relaxation between +40% and −40% of the bulk interlayer spacing had no significant effect of the adsorbate modes (see Fig. 16). The best fit was obtained for an oxygen height of 0.92(224) Å, determined primarily by the oxygen perpendicular and parallel mode frequencies near $\bar{\Gamma}$. In fact, a two-parameter fit to our data varying only the oxygen height and nickel-oxygen force constant gave a height of 0.93(2) Å, assuming no reconstruction. Although it was probably unnecessary, and slightly increased the amount of time required to fit the data, each parameter was determined to at least five significant figures by fitting the data to within less than 0.001 meV. Since the experimental peak positions cannot be determined to this accuracy nothing is gained over a fit within 0.1 meV, but it

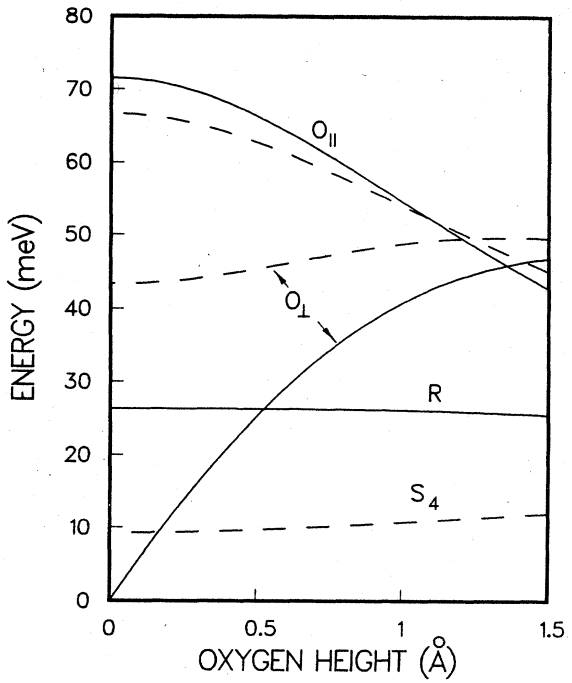

FIG. 8. Variation of surface-mode energies with height of $c(2\times2)$O above Ni(100) surface at $\bar{\Gamma}$ (solid lines) and $\bar{X}$ (dashed lines). All other parameters are fixed at values determined by best fit to five data points, the oxygen is located above the fourfold hollow site, and the nickel surface is relaxed outward 5.2% based on Rutherford backscattering data (Ref. 27). The central-force constants in this model are inversely proportional to the square of the distance between atoms, so the nickel-oxygen force constant becomes slightly stronger as the oxygen approaches the nickel plane.

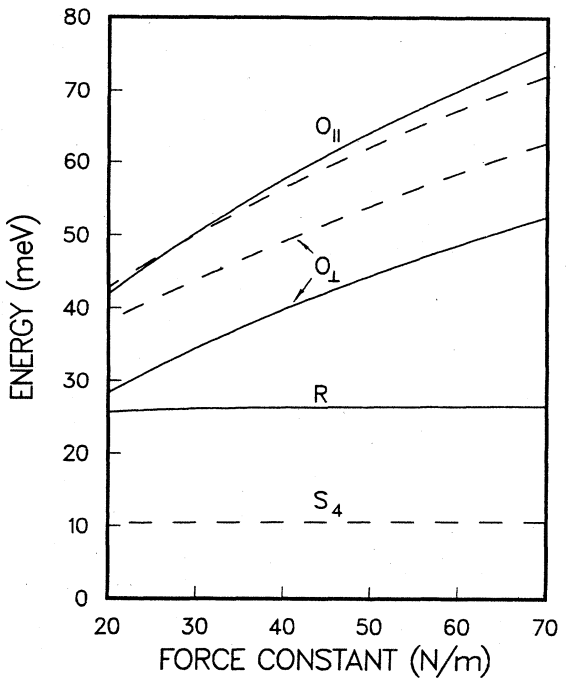

FIG. 9. Variation of surface-mode energies of $c(2\times2)$O/Ni(100) with nickel-oxygen nearest-neighbor central-force constant at $\bar{\Gamma}$ (solid lines) and $\bar{X}$ (dashed lines). Oxygen height fixed at 0.92(224) Å, surface relaxed 5.2%.

made more obvious the dependence (often weak) of each mode on each parameter.

Once the seven-parameter calculation was fit to the five data points each parameter was varied over a large range to determine that parameter's effect on the frequencies at $\bar{\Gamma}$ and $\bar{X}$ and to see if, in fact, a best fit had been obtained. Figure 8 displays the effect on the surface modes of varying the oxygen height with all other parameters held fixed (in our calculation the force constants depend on the distance between atoms so the nickel-oxygen force constant is also changing a small amount; the calculation does not require the force constant to be related to the distance so this is an artifact of this implementation of our program). The oxygen vibrational modes at $\bar{\Gamma}$ show the greatest variation with height and, more importantly, the mode polarized perpendicular to the surface is monotonically increasing while the mode polarized parallel to the surface is monotonically decreasing. It should be pointed out that the two oxygen modes polarized parallel to the surface are degenerate at $\bar{\Gamma}$ and $\bar{X}$ due to the high symmetry of these points as well as the symmetry of the fourfold hollow site, but they should not be degenerate at other points in the surface Brillouin zone and are not degenerate in our calculations, being split by 0.7 meV at $q_{\parallel}\approx0.6$ as shown in Fig. 19. However, the Green's-function calculations of Rahman *et al.*[5] indicate that they are degenerate at all points along $\bar{\Delta}$, implying that there may have been a mistake in their calculations.

Figure 9 shows that the frequency of both of the oxygen modes increases as a function of the nickel-oxygen nearest-neighbor central-force constant, so that there can only be one choice of height and force constant which fit both oxygen modes simultaneously if only first-nearest-neighbor central forces are allowed. This is due to the relationship between the adsorbate bond angle and the frequencies perpendicular and parallel to the surface. For an atom in a fourfold hollow site, the ratio of the perpendicular mode frequency to the parallel mode frequency is $\sqrt{2}\cot(\alpha)$, assuming the substrate atoms are frozen in space (the infinite-substrate-mass approximation), where α is the angle between the adsorbate-substrate bond and the surface normal. It is interesting to note that the infinite-substrate-mass approximation fits our calculated frequencies better than when the first correction for the finite-substrate mass[28] is included, until the adsorbate is very high above the surface (see Fig. 10). If second-nearest-neighbor or angle-bending interactions with the adsorbate are nonzero, virtually any relationship between the frequencies of the adsorbate modes perpendicular and parallel to the surface can be obtained. This is why it is important to begin a lattice-dynamical analysis of a structural parameter (such as the adsorbate height) with a general force-constant model and use experimental constraints to arrive at the set of parameters which best fit the data. Figure 11 shows that the nickel-oxygen second-nearest-neighbor central-force constant affects only the oxygen mode polarized perpendicular to the surface and that the dispersion of this mode is greatest when this force con-

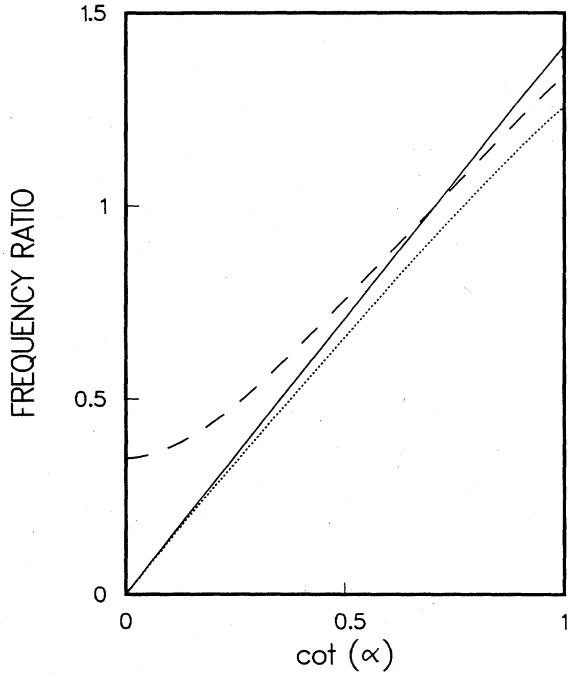

FIG. 10. Ratio of adsorbate frequency perpendicular to the surface to frequency parallel to the surface vs the cotangent of the angle between the adsorbate-substrate bond and the surface normal. Solid line, infinite-substrate-mass approximation; dashed line, infinite-substrate-mass approximation plus first-order correction for finite-substrate mass; dotted line, exact relationship based on our finite-slab calculations.

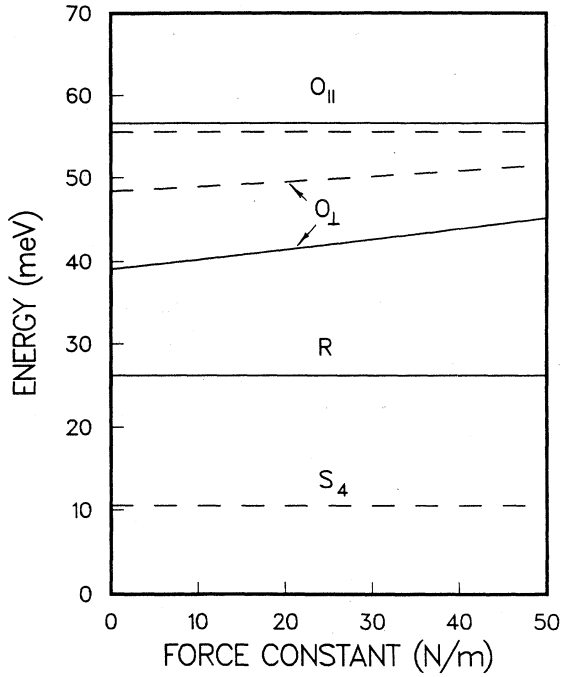

FIG. 11. Variation of surface-mode energies of $c(2\times2)$O/Ni(100) with nickel-oxygen second-nearest-neighbor central-force constant at $\bar{\Gamma}$ (solid lines) and $\bar{X}$ (dashed lines). Oxygen height fixed at 0.92(224) Å, surface relaxed 5.2%.

stant is zero; the large dispersion of this mode in the data is thus best fit when there is no second-nearest-neighbor nickel-oxygen interaction. The same conclusion holds for the nickel-oxygen-nickel angle-bending force constant (see Fig. 12), so that we do, indeed, have only first-nearest-neighbor central forces in the model with the best fit, guaranteeing there will only be one oxygen height possible.

The dispersion of the oxygen mode polarized parallel to the surface is adjusted with the oxygen-oxygen nearest-neighbor central-force constant (see Fig. 13), which has a very small affect on the S_4 surface phonon (the Rayleigh wave), and absolutely no affect on the surface modes at $\bar{\Gamma}$. The dispersion of the S_4 surface phonon is primarily determined by the (surface nickel)-(second-layer nickel) nearest-neighbor central-force constant, which affects all of the surface modes to a small degree (see Fig. 14). The nickel surface-resonance mode frequency can be adjusted up or down by changing the (surface nickel)-(surface nickel) nearest-neighbor central-force constant (see Fig. 15). While this parameter also affects the dispersion of the oxygen mode polarized perpendicular to the surface, the force constant required to fit the perpendicular mode dispersion would be much greater than the bulk nickel-nickel nearest-neighbor central-force constant, and this does not seem physically reasonable in addition to producing the wrong frequency of the surface-resonance mode.

As mentioned earlier, variation of the surface relaxation (and simultaneously the surface nickel to second-layer

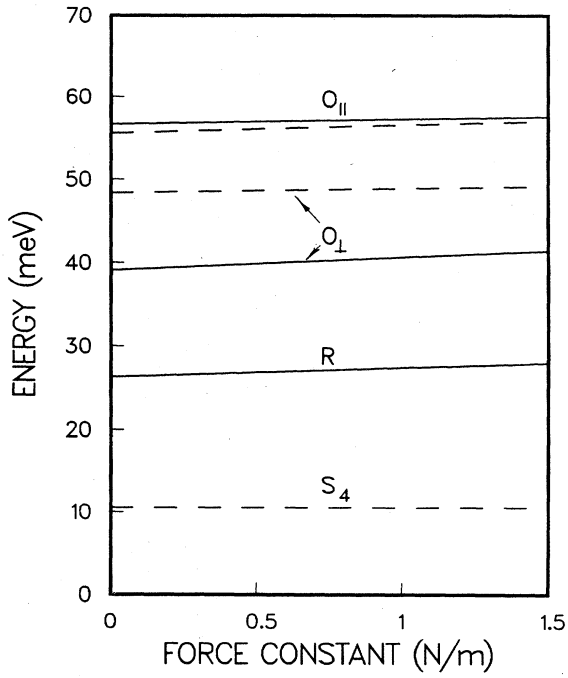

FIG. 12. Variation of surface-mode energies of $c(2\times2)$O/Ni(100) with nickel-oxygen-nickel angle-bending force constant at $\bar{\Gamma}$ (solid lines) and $\bar{X}$ (dashed lines). Oxygen height fixed at 0.92(224) Å, surface relaxed 5.2%.

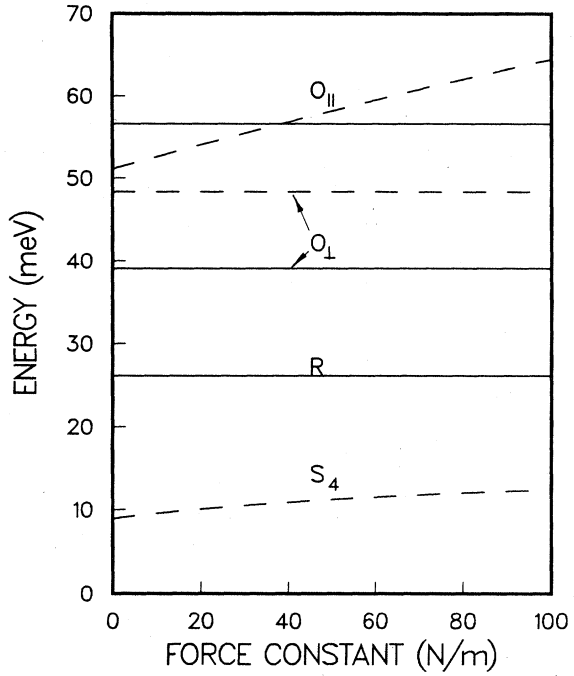

FIG. 13. Variation of surface-mode energies of $c(2\times2)$O/Ni(100) with oxygen-oxygen nearest-neighbor central-force constant at $\bar{\Gamma}$ (solid lines) and $\bar{X}$ (dashed lines). Oxygen height fixed at 0.92(224) Å, surface relaxed 5.2%.

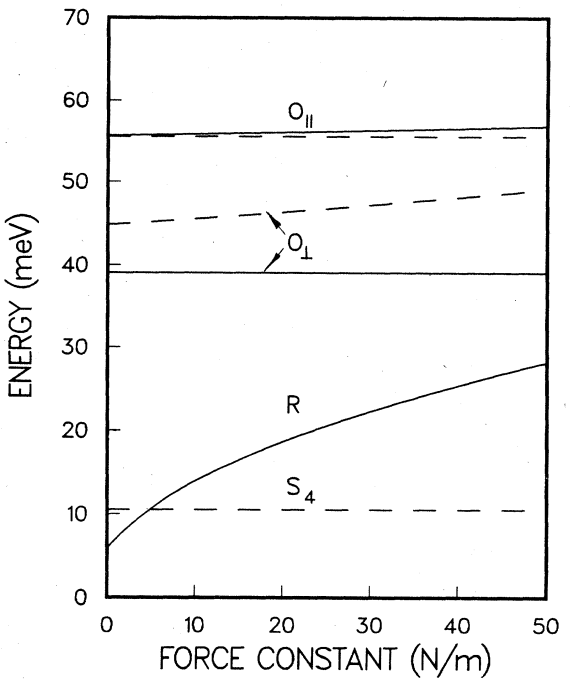

FIG. 15. Variation of surface-mode energies of $c(2\times2)$O/Ni(100) with (surface nickel)-(surface nickel) nearest-neighbor central-force constant at $\bar{\Gamma}$ (solid lines) and $\bar{X}$ (dashed lines). Oxygen height fixed at 0.92(224) Å, surface relaxed 5.2%.

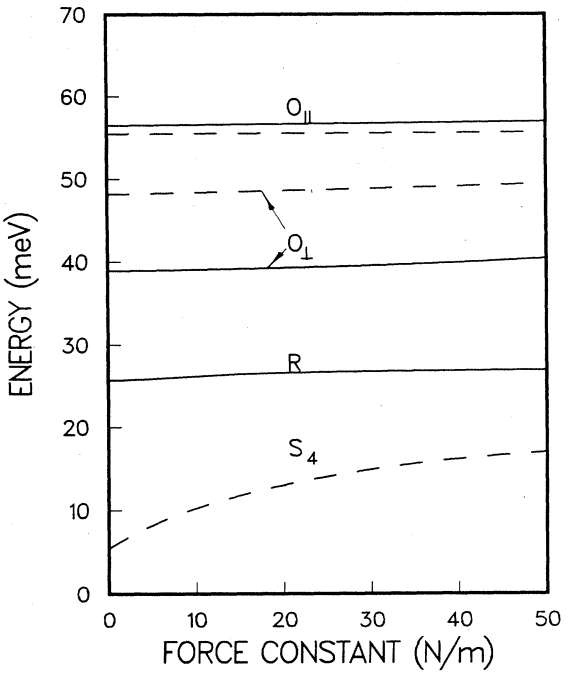

FIG. 14. Variation of surface-mode energies of $c(2\times2)$O/Ni(100) with (surface nickel)-(second-layer nickel) nearest-neighbor central-force constant at $\bar{\Gamma}$ (solid lines) and $\bar{X}$ (dashed lines). Oxygen height fixed at 0.92(224) Å, surface relaxed 5.2%.

nickel force constant) has little affect on any of the surface modes (see Fig. 16). Each mode is therefore associated with one or two parameters, so it is possible to fit all modes simultaneously in a fairly straightforward manner. We are therefore confident that we have arrived at the best fit possible within the constraints of the parameter set we have chosen. Assuming adsorption in the fourfold hollow site, the EELS data and a parametrized lattice-dynamical calculation give a precise determination of the adsorbate height in agreement with the original LEED calculation of 0.9 ± 0.1 Å, and similarly within the uncertainty of the results of the other experimental techniques.

The surface-resonance mode is the most difficult mode to characterize because it is not a single mode but a collection of modes. Some of these modes are even under reflection through the mirror plane passing through the oxygen atoms, while others are odd. The even modes have the oxygen motion in the mirror plane while the odd modes have the oxygen motion perpendicular to the mirror plane and parallel to the surface, consequently the dipole spectral density parallel to the surface and in the scattering plane must be zero for odd modes but may be nonzero for even modes. All of the surface-resonance modes have the surface nickel atoms vibrating predominantly parallel to the surface with components both parallel and perpendicular to the mirror plane. The even modes exhibit smaller vibrational amplitudes of the nickel atoms parallel to the surface and in the scattering plane than the odd modes, so the corresponding impact spectral density is larger for the odd modes than the even modes. The odd modes would therefore appear strongest if the

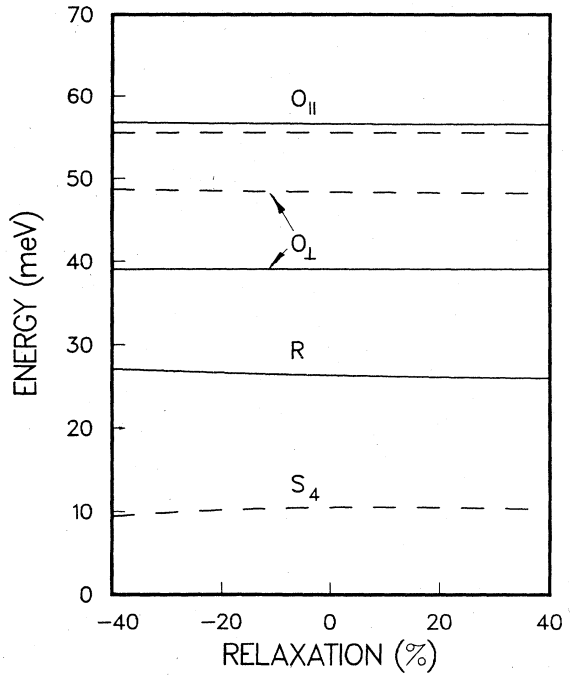

FIG. 16. Variation of surface-mode energies of $c(2\times2)$O/Ni(100) with surface relaxation (+ outward; − inward) at $\bar{\Gamma}$ (solid lines) and $\bar{X}$ (dashed lines). Oxygen height fixed at 0.92(224) Å. The (surface nickel)-(second-layer nickel) nearest-neighbor central force constant is also varying due to our Lennard-Jones model.

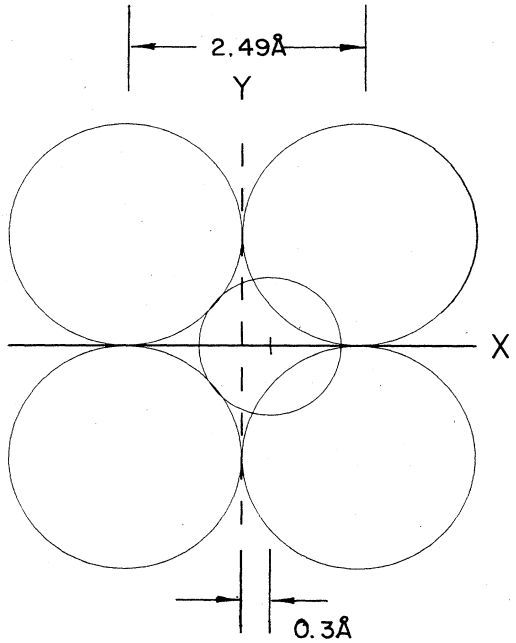

FIG. 17. Pseudobridge site proposed by Demuth *et al.* (Ref. 12) for $c(2\times2)$O/Ni(100). The oxygen is 0.8 Å above the surface and displaced 0.3 Å from the fourfold hollow site towards a bridge site. The nearest-neighbor distance in nickel is 2.49 Å.

scattering is predominantly associated with the potentials of the nickel atoms while the even modes would appear strongest if the scattering is from the oxygen atom potentials (assuming from kinematical scattering arguments that only vibrations parallel to the scattering plane, which is along the mirror plane, can be detected). The even modes disperse upwards in energy away from $\bar{\Gamma}$ while the odd modes are nearly flat. The observed dispersion away from $\bar{\Gamma}$ is initially flat and then dips downward in energy, so that the odd modes give a slightly better fit. The odd modes are much more localized to the surface than the even modes, which are nearly uniform throughout the slab. Consequently, when the thickness of the slab is increased from 13 to 27 layers the spectral densities of the even modes decrease much more than the spectral densities of the odd modes, due to the normalization of the eigenvectors. All of the available evidence seems to point to the odd modes as the source of the observed resonance mode, which would contradict the impact-scattering selection rule[13] which predicts that odd modes should be unobservable when the electron detector is in the scattering plane formed by the incident electron beam and the surface normal (Rahman *et al.*[5,27] assumed only even modes could be observed). This demonstrates the value of knowing the entire eigenvector associated with a given mode, which apparently is more difficult to determine with the Green's-function method.

Although the adsorption sites discussed so far have been highly symmetric, the finite-slab calculation easily handles asymmetric adsorption sites as well. For example, Demuth[12] has proposed a pseudobridge site for the oxygen atoms in the $c(2\times2)$ overlayer on Ni(100) 0.3 Å off center from the fourfold hollow site at a height of 0.8 Å (see Fig. 17). On the basis of group theory, the reduced symmetry of the pseudobridge site should give rise to two peaks observable in specular EELS. This is because the oxygen mode parallel to the surface and parallel to the displacement from the fourfold hollow site will also have some amplitude perpendicular to the surface (the oxygen mode perpendicular to the surface will also have a small component parallel to the surface); we will henceforth refer to this predominantly parallel oxygen mode as the pseudo parallel mode. When the oxygen is laterally displaced perpendicular to the scattering plane all three oxygen modes should be observable in off-specular EELS since there is no mirror-plane or rotation symmetry on which to base impact-scattering selection rules. If the oxygen is laterally displaced along the scattering plane then the scattering plane is still a mirror plane and only one of the oxygen parallel modes will be observable in off-specular EELS (the pseudo parallel mode). Rahman *et al.*[5] performed periodic cluster calculations (a finite-slab calculation with one nickel layer)[14] instead of their usual Green's-function calculations for $c(2\times2)$O/Ni(100) with the oxygen in the pseudobridge site at a height of 0.9 Å instead of 0.8 Å. Rahman *et al.* thus did not actually test Demuth's proposed geometry. Rahman *et al.* used two different force constants for the long and short nickel-oxygen bonds, varied the ratio F of these two force constants while simultaneously fitting the oxygen perpendicular mode at $\bar{\Gamma}$, and reported the oxygen perpendicular

and parallel mode frequencies at various points along $\bar{\Delta}$, along with the ratio R of the pseudo parallel mode's components perpendicular and parallel to the surface (equivalent to the tangent of the angle formed by the oxygen displacement and the surface). Rahman *et al.* found that for large ratios of the nickel-oxygen force constants that the perpendicular component of the pseudo parallel mode becomes very large at $\bar{\Gamma}$ and hence this mode should be easily observable in specular EELS. However, the parallel mode frequencies do not fit the data for these large force-constant ratios, and they do not report any values for the dipole spectral density to compare the pseudo parallel mode with the pseudoperpendicular mode.

We have performed finite-slab calculations for oxygen in the pseudobridge site at a height of 0.8 Å which indicate that the pseudo parallel mode of oxygen does, indeed, have a small dipole spectral density perpendicular to the surface at $\bar{\Gamma}$ when $R=0.218$ and $F=1.485$, but it is 40 times smaller than the dipole spectral density of the predominantly perpendicularly polarized oxygen mode. This is not inconsistent with the specular EELS data we have taken, which show a very weak shoulder near 55 meV on the side of the 39-meV peak corresponding to the perpendicular mode. However, this could also be due to small domains of $p(2\times2)$O coexisting with the $c(2\times2)$O domains. In order to fit both the oxygen perpendicular mode and pseudo parallel mode simultaneously at a height of 0. 8 Å, it is necessary to introduce an oxygen interaction with the nickel atom underneath it in the second layer. The strength of the oxygen interaction with the second layer could be reduced to zero by putting the oxygen height somewhere near the 0.92 Å determined for adsorption ion the fourfold hollow site. This is because the oxygen parallel mode frequencies increase as the oxygen atom approaches the nickel surface while the surface nickel-oxygen force constants are adjusted to fit the oxygen perpendicular mode frequency. By including the oxygen interaction with the second layer (where the bond is nearly perpendicular to the surface), the oxygen interaction with the first layer can be reduced when fitting the oxygen perpendicular mode frequency, simultaneously decreasing the frequency of the oxygen parallel modes. This may explain why Rahman *et al.*[5] did not use 0.8 Å for the oxygen height in their periodic cluster calculation (they did not have a second nickel layer with which the oxygen could interact). We did not attempt to include any angle-bending interactions in our calculations because this would introduce at least three additional parameters for which no reasonable values are known (we have already introduced one additional parameter by having different force constants for the long and short bonds between the oxygen atom and the surface nickel atoms), otherwise the calculations were identical to those for adsorption in the fourfold hollow site with the oxygen height fixed instead of variable. The two parallel modes of the oxygen are split by at most 3 meV (see Fig. 18), which would be extremely difficult to detect with a resolution of 4 meV, and is within the spread of the experimental data (see Fig. 3 inset). For comparison, the surface modes of $c(2\times2)$O in the fourfold hollow site of both even and odd symmetry (under reflection in the scattering plane parallel to $\bar{\Delta}$) are

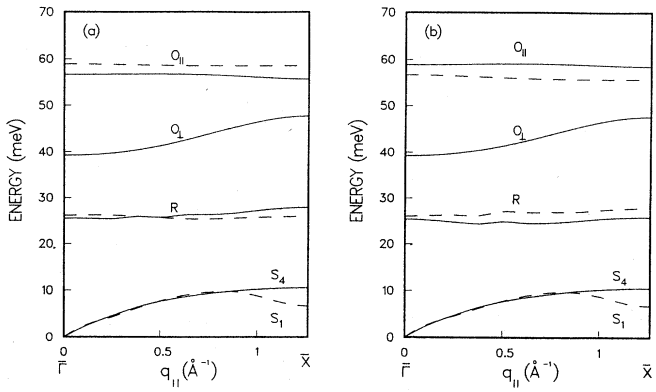

FIG. 18. Calculated surface-mode dispersion curves for $c(2\times2)$O/Ni(100) with oxygen adsorbed in pseudobridge sites. Solid lines are modes polarized predominantly perpendicular to the surface or parallel to the surface and in the scattering plane (shear vertical and longitudinal modes), while dashed lines are parallel to the surface and perpendicular to the scattering plane (shear horizontal modes). The dispersion curves for oxygen displacement from the hollow site in the directions parallel and perpendicular to $\mathbf{q}_{\parallel}$ are shown in (a) and (b), respectively. In the latter case (b) the scattering plane is not a mirror plane to all surface modes are observable, while in the former case (a) shear horizontal modes are not observable according to impact-scattering selection rules (Ref. 13).

shown in Fig. 19. The only evidence against the pseudobridge site in terms of the EELS data is that the S_1 surface phonon should be observable in those domains where the oxygen atom is displaced from the fourfold hollow site in the direction perpendicular to the scattering plane, but the largest splitting between the S_1 and S_4 surface phonons is less than 4 meV (at $\bar{X}$) and this would also be difficult to measure. Consequently, the pseudobridge site cannot be discounted on the basis of symmetry and group-theoretical arguments. The fact that the observed S_4 dispersion curve dips near $\bar{X}$ may in fact be a result of the superposition of the S_1 and S_4 peaks, since the former has a similar dip in the calculated dispersion curves while the latter does not. If this is correct then one must conclude that the $c(2\times2)$O adsorption is, in fact, at the pseudobridge site. However, our judgment is that the best experimental data is presently unable to distinguish between the fourfold hollow and pseudobridge sites.

Szeftel and Lehwald[29] have reported dispersion curves for $p(2\times2)$O/Ni(100) and claim that the frequencies of the oxygen modes polarized perpendicular and parallel to the surface are consistent with an oxygen height of 0.88 Å, using the finite-mass correction formula mentioned earlier.[28] Using their values for the frequencies, we have performed slab calculations which indicate an oxygen height of 0.6688 Å, which is inconsistent with the accepted value of 0.9 Å. We find from our calculations that if the oxygen is at 0.9 Å, the oxygen mode polarized parallel to the surface should be found at 67.9 meV (unfortunately close to the NiO phonon mode at 69 meV) and not at 79.4 meV as reported (the perpendicular mode has been measured in specular EELS at 53.3 meV). Our own EELS experiments with $p4g(2\times2)$ carbon overlayers on Ni(100)

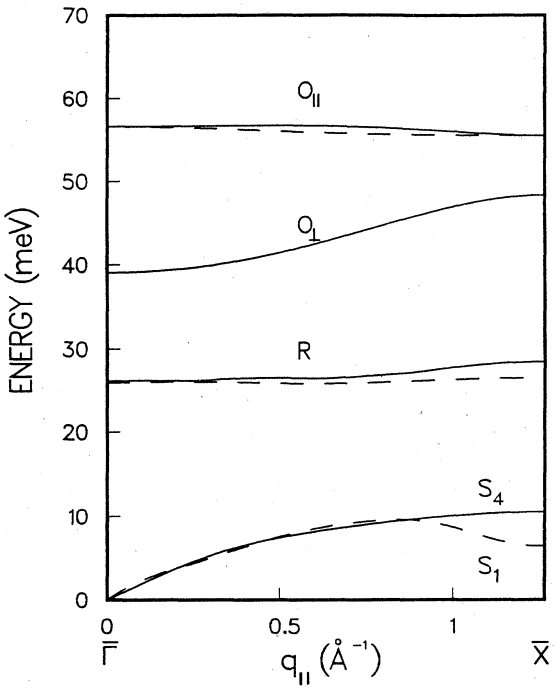

FIG. 19. Calculated surface-mode dispersion curves for $c(2\times2)$O/Ni(100) with oxygen adsorbed in fourfold hollow sites. Solid lines are modes polarized predominantly perpendicular to the surface or parallel to the surface and in the scattering plane (shear vertical and longitudinal modes), while dashed lines are parallel to the surface and perpendicular to the scattering plane (shear horizontal modes). Shear horizontal modes are not observable according to impact-scattering selection rules (Ref. 13).

indicated a peak near 80 meV in off-specular geometry, which our calculations for a $p(2\times2)$ carbon overlayer show are consistent with the LEED determined height of 0.1 to 0.2 Å.[30] This demonstrates the ability of the finite-slab model to check the consistency of proposed structural models with measured vibrational spectra.

CONCLUSIONS

Using finite-slab calculations one can determine adsorption sites and adsorbate heights from surface vibrational spectra alone. Spectral densities obtained with the slab method are as sensitive to variations in the adsorbate site and other structural parameters as those obtained by the Green's-function method. Even with limited data, as available in specular EELS, the calculations are able to determine the adsorption site when the adsorbate height is known and there is more than one loss peak in the spectrum. The calculations can also serve as a check on proposed structural models by determining if all of the vibrational data is consistent with the model using reasonable force constants. The calculation is straightforward, can be performed on any modest-sized computer, and can be mastered in a very short time, allowing anyone with the inclination to interpret their own surface vibrational spectra.

APPENDIX

We seek solutions of the eigenvalue problem

$$\omega_i^2(\mathbf{q}_{||})e_{i\alpha}(\mathbf{q}_{||}\,|\,k)=\sum_{k'\beta}D_{\alpha\beta}(\mathbf{q}_{||}\,|\,kk')e_{i\beta}(\mathbf{q}_{||}\,|\,k')\ , \quad \text{(A1)}$$

where i labels the $3N$ solutions, k and k' label the N atoms in the unit cell, $\mathbf{q}_{||}$ is the two-dimensional wave vector, α and β are Cartesian coordinates x, y, or z, D is the dynamical matrix, and the eigenvectors $\mathbf{e}_i(\mathbf{q}_{||})$ satisfy the usual orthonormality and closure relations. The vibrational amplitude of atom k in unit cell l for mode i and wave vector $\mathbf{q}_{||}$ is related to its corresponding eigenvector by

$$u_{i\alpha}(\mathbf{q}_{||}\,|\,k,l)=\frac{e_{i\alpha}(\mathbf{q}_{||}\,|\,k)}{(m_k)^{1/2}}e^{i\mathbf{q}_{||}\cdot\mathbf{R}_{||}(l)}\ , \quad \text{(A2)}$$

where m_k is the mass of atom k and $\mathbf{R}_{||}(l)$ is the two-dimensional lattice translation vector between cell l and the fundamental unit cell ($l=0$). The dynamical matrix D is defined by

$$D_{\alpha\beta}(\mathbf{q}_{||}\,|\,kk')=\frac{1}{(m_km_{k'})^{1/2}}\sum_l\Phi_{\alpha\beta}(0k;lk')e^{i\mathbf{q}_{||}\cdot\mathbf{R}_{||}(l)}\ , \quad \text{(A3)}$$

where

$$\Phi_{\alpha\beta}(0k;lk')=\left[\frac{\partial^2\Phi}{\partial u_\alpha(0k)\partial u_\beta(lk')}\right]_{\mathbf{u}(0k)=\mathbf{u}(lk')=0}\ , \quad \text{(A4)}$$

and Φ is the total slab potential energy. If r is the distance between atom k in cell 0 and atom k' in cell l and $\phi(0k;lk')$ is the corresponding pair potential, then define

$$\phi_{\alpha\beta}(0k;lk')=\frac{r_\alpha r_\beta}{r^2}\frac{\partial^2\phi(0k;lk')}{\partial r^2}\ , \quad \text{(A5)}$$

where r_α is the α component of $\mathbf{r}$ from atom k to atom k'. It can be shown that

$$\Phi_{\alpha\beta}(0k;lk')=-\phi_{\alpha\beta}(0k;lk')+\delta_{0,l}\delta_{k,k'}\sum_{l'k''}\phi_{\alpha\beta}(0k;l'k'')\ . \quad \text{(A6)}$$

From (7) and (10) it follows that

$$D_{\alpha\beta}(\mathbf{q}_{||}\,|\,kk)=\frac{-1}{m_k}\sum_l\left[\phi_{\alpha\beta}(0k;lk)e^{i\mathbf{q}_{||}\cdot\mathbf{R}_{||}(l)}-\sum_{k'}\phi_{\alpha\beta}(0k;lk')\right] \quad \text{(A7)}$$

and

$$D_{\alpha\beta}(\mathbf{q}_{||}\,|\,kk')=\frac{-1}{(m_km_{k'})^{1/2}}\sum_l\phi_{\alpha\beta}(0k;lk')e^{i\mathbf{q}_{||}\cdot\mathbf{R}_{||}(l)}\ \text{if}\ k'\neq k\ . \quad \text{(A8)}$$

In the Lennard-Jones model

$$\phi_{\alpha\beta}(0k;lk')=\frac{72\epsilon r_\alpha r_\beta}{r^4}\ , \quad \text{(A9)}$$

while in a central-force-constant model with force constant K,

$$\phi_{\alpha\beta}(0k;lk')=\frac{Kr_\alpha r_\beta}{r^2} . \quad \text{(A10)}$$

All results presented in the present paper were obtained using the model of Eq. (A9). In a nearest-neighbor model l is summed over the nine unit cells with the fundamental unit cell in the center. This is most easily accomplished by replacing l with two indices summed from -1 to 1, corresponding to the coefficients of the two primitive translation vectors between the fundamental unit cell and one of the nine cells in the sum over l. If k runs from 1 to N, then $D_{\alpha\beta}(\mathbf{q}_{||}\,|\,kk')$ can be configured as a $3N\times 3N$ matrix by letting $\alpha=1,2,3$ correspond to x,y,z and defining

$$D_{\alpha+3(k-1),\beta+3(k'-1)}(\mathbf{q}_{||})=D_{\alpha\beta}(\mathbf{q}_{||}\,|\,kk') . \quad \text{(A11)}$$

The calculation of the dynamical matrix is thus reduced to two sums over the N atoms in the unit cell, two sums from -1 to 1, and two sums from 1 to 3.

Once the dynamical matrix is formed, standard library routines are used to solve for the eigenvalues and eigenvectors (complex if not at a high-symmetry point). The IMSL library routines we used on our VAX 11/780 are VCVTCH and EIGCH. The EISPACK library routines we used on our CDC Dual Cyber 170/750 are HTRIDI, IMTQL2, and HTRIBK.

ACKNOWLEDGMENTS

We are pleased to acknowledge many helpful discussions with F. W. deWette and B. Firey, and we thank F. W. deWette for the computer program which served as the basis for the calculations described in this paper. This work was sponsored by the Air Force Office of Scientific Research under Grant No. AFOSR-83-0131.

[1]G. Brusdeylins, R. B. Doak, and J. P. Toennies, Phys. Rev. B **27**, 3662 (1983); R. B. Doak and J. P. Toennies, Surf. Sci. **117**, 1 (1982); G. Benedek, J. Electron Spectrosc. Relat. Phenom. **29**, 187 (1983).

[2]R. B. Doak, U. Harten, and J. P. Toennies, Phys. Rev. Lett. **51**, 578 (1983); G. J. M. Horne and D. R. Milles, Phys. Rev. Lett. **41**, 511 (1978); M. Cates and D. R. Milles, J. Electron Spectrosc. Relat. Phenom. **30**, 157 (1983); Phys. Rev. B **28**, 3615 (1983).

[3]S. Lehwald, J. M. Szeftel, H. Ibach, T. S. Rahman, and D. L. Mills, Phys. Rev. Lett. **50**, 518 (1983).

[4]R. L. Strong and J. L. Erskine, Rev. Sci. Instrum. **55**, 1304 (1984); Phys. Rev. Lett. **54**, 346 (1985); Bull. Am. Phys. Soc. **27**, 372 (1982).

[5]T. S. Rahman, D. L. Mills, J. E. Black, J. M. Szeftel, S. Lehwald, and H. Ibach, Phys. Rev. B **30**, 589 (1984).

[6]J. B. Pendry, *Low Energy Electron Diffraction* (Academic, London, 1974).

[7]M. A. Van Hove and S. Y. Tong, *Surface Crystallography by LEED* (Springer, Berlin, 1979).

[8]F. Soria, V. Martinez, M. C. Munoz, and J. L. Sacedon, Phys. Rev. B **24**, 6926 (1981).

[9]S. Y. Tong and K. H. Lau, Phys. Rev. B **25**, 7382 (1982).

[10]J. L. Erskine and R. L. Strong, Phys. Rev. B **25**, 5547 (1982).

[11]R. L. Strong, B. Firey, F. W. deWette, and J. L. Erskine, Phys. Rev. B **26**, 3483 (1982).

[12]J. E. Demuth, N. J. Dinardo, and G. S. Cargill, Phys. Rev. Lett. **50**, 1373 (1983).

[13]S. Y. Tong, C. H. Li, and D. L. Mills, Phys. Rev. B **24**, 806 (1981); C. H. Li, S. Y. Tong, and D. L. Mills, Phys. Rev. Lett. **44**, 407 (1980).

[14]J. E. Black, Surf. Sci. **116**, 240 (1982).

[15]R. E. Allen, G. P. Alldredge, and F. W. deWette, Phys. Rev.B **4**, 1648 (1971); **4**, 1661 (1971); **4**, 1682 (1971).

[16]A. A. Maradudin, E. W. Montroll, G. H. Weiss, and I. P. Ipatova, *Theory of Lattice Dynamics in the Harmonic Approximation,* 2nd ed. (Academic, New York, 1971).

[17]P. N. Keating, Phys. Rev. **145**, 637 (1965).

[18]E. Evans and D. L. Mills, Phys. Rev. B **5**, 4126 (1972).

[19]T. S. Rahman, J. E. Black, and D. L. Mills, Phys. Rev. B **25**, 883 (1982).

[20]T. S. Rahman, D. L. Mills, and J. E. Black, Phys. Rev. B **27**, 4059 (1983).

[21]H. Ibach and D. Bruchmann, Phys. Rev. Lett. **44**, 36 (1980).

[22]J. E. Demuth, D. W. Jepsen, and P. M. Marcus, Surf. Sci. **53**, 501 (1975).

[23]T. Upton and W. A. Goddard, Phys. Rev. Lett. **46**, 1635 (1981).

[24]J. E. Demuth, D. W. Jepsen, and P. M. Marcus, Phys. Rev. Lett. **31**, 540 (1973).

[25]Surface extended x-ray absorption fine structure, He diffraction, energy-dependent photoelectron diffraction, surface electron-energy-loss fine structure, and near-edge x-ray absorption fine-structure experiments.

[26]J. M. Szeftel, S. Lehwald, H. Ibach, T. S. Rahman, J. E. Black, and D. L. Mills, Phys. Rev. Lett. **51**, 268 (1983).

[27]J. W. M. Frenken, J. F. van der Veen, and G. Allan, Phys. Rev. Lett. **51**, 1876 (1983).

[28]H. Ibach and D. L. Mills, *Electron Energy Loss Spectroscopy and Surface Vibrations* (Academic, New York, 1982), p. 149.

[29]J. M. Szeftel and S. Lehwald, Surf. Sci. **143**, 11 (1984).

[30]J. H. Onuferko, D. P. Woodruff, and B. W. Holland, Surf. Sci. **87**, 357 (1979).